OPEN ACCESS

Nonlinear quantum metrology using coupled nanomechanical resonators

New Journal of Physics
The open-access journal for physics

Nonlinear quantum metrology using coupled nanomechanical resonators

M J Woolley[1], **G J Milburn**[1] **and Carlton M Caves**[1,2]
[1] Department of Physics, School of Physical Sciences, University of Queensland, St Lucia, Queensland 4072, Australia
[2] Department of Physics and Astronomy, MSC07-4220, University of New Mexico, Albuquerque, NM 87131-0001, USA
E-mail: caves@info.phys.unm.edu

New Journal of Physics **10** (2008) 125018 (13pp)
Received 29 April 2008
Published 4 December 2008
Online at http://www.njp.org/
doi:10.1088/1367-2630/10/12/125018

Abstract. We consider a nanomechanical analogue of a nonlinear interferometer, consisting of two parallel, flexural nanomechanical resonators, each with an intrinsic Duffing nonlinearity and with a switchable beamsplitter-like coupling between them. We calculate the precision with which the strength of the nonlinearity can be estimated and show that it scales as $1/n^{3/2}$, where n is the mean phonon number of the initial state. This result holds even in the presence of dissipation, but assumes the ability to make measurements of the quadrature components of the nanoresonators.

Contents

1. Introduction

High-precision measurement is an essential component of any advanced technology, be it classical or quantum. In the case of the emerging quantum technologies, however, constraints on our ability to make precise measurements are imposed by the Heisenberg uncertainty principle. It is often the case that the measurement objective is simply to estimate a single parameter of the Hamiltonian of a system [1]. For example, in atomic clocks the objective is to estimate the resonant frequency of a given electronic transition [2]. In the case of an optical interferometer, the objective is to estimate an optical phase shift produced by some mechanism of interest, which changes the relative path length. As the parameter varies, the dynamics of the system changes, and precise determination of the parameter requires that the change in the dynamics of the system be resolvable with sufficient sensitivity to the parameter.

The precision with which the parameter can be determined depends on the initial state of the system, the nature of the Hamiltonian describing the system's evolution, and the measurements to be performed on the system. Most work on parameter estimation assumes that system quanta are coupled independently to the parameter, meaning that the coupling is quadratic in the field variables, which leads to equations of motion that are linear in the field variables. For such linear couplings, the optimal precision in a parameter estimate scales as $1/n$, where n is the number of system quanta used in the measurement, a scaling known as the Heisenberg limit [3]. Achieving the Heisenberg limit with a linear coupling requires using an entangled initial state [4]. If one is restricted to using product states, then a linear coupling can only achieve a $1/n^{1/2}$ scaling, which is called the shot-noise limit or the standard quantum limit.

It was recently shown that quantum parameter estimation with scaling better than $1/n$ could be attained by using a coupling to the parameter that is *nonlinear* in field variables [5]; such super-Heisenberg scalings can be obtained even with an initial product state [6]. The use of product states, as opposed to entangled states, circumvents the difficulty of creating the entangled states and also makes the scheme considerably more robust against the deleterious effects of decoherence.

In a related development, a measurement of a phase shift of an optical field [7], using an adaptive measurement scheme that requires no entanglement, has achieved a Heisenberg-limited sensitivity in terms of number of interactions of photons with the phase shifter, rather than just the number of photons. The number of interactions each photon undergoes is a discrete version of the coherent evolution time in most metrology protocols. Increasing the coherent evolution time, as in the experiment of [7], is generally a good strategy for improving sensitivity, but it is relatively easy to do, and its utility is limited by the need to determine a parameter before it changes (i.e. with a certain bandwidth) or by decoherence. Some quantum metrology literature (see, for example [3, 8, 9]) regards the number of interactions as the relevant resource. In the system we consider here, the number of quanta and the number of interactions each quantum experiences are not equivalent resources. Hence, we use the number of quanta as the relevant resource.

Flexural nanomechanical resonators have an intrinsic *Duffing nonlinearity* due to extension on bending [10]; technology is progressing toward the point where such resonators can be cooled to near their quantum ground state [11]. Thus nanoresonators might provide a system in which parameter estimation beyond the $1/n$ Heisenberg limit could be demonstrated, in this case measurement of the nonlinear coefficient for the Duffing nonlinearity. Other candidates for the first experimental demonstration of super-Heisenberg scalings in parameter estimation

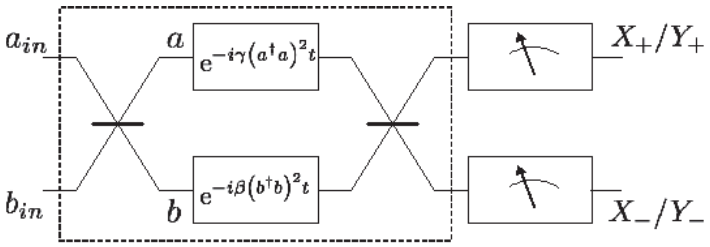

Figure 1. Quantum circuit representation of nonlinear nanoresonator interferometer. The input nanoresonator modes experience a pulsed beamsplitter-like interaction, evolve according to a nonlinear Hamiltonian, and the beamsplitter-like interaction is then pulsed on again. We assume that measurements can be made of either the X or the Y quadrature, of one or both output modes (denoted '+' and '−'). Though not shown in the circuit, we have also considered the effect of dissipation accompanying the nonlinear evolution.

include the measurement of phase in a nonlinear optics setting [12]–[14], the measurement of a magnetic field in atomic magnetometry [15], and the measurement of atomic scattering strength in coupled Bose–Einstein condensates [16]–[18].

Quite apart from any fundamental considerations, the ability to make high-precision measurements of the Duffing nonlinearity of a nanomechanical resonator might be of considerable practical interest. The Duffing nonlinearity of a nanomechanical resonator is an expression of the applied strain [19]. Nonlinear micro-electromechanical systems (MEMS) have already been used to make highly sensitive mechanical strain sensors and accelerometers, with applications to engineering and biomedical systems [20]. High-precision measurements of the Duffing nonlinearity would also have implications for ultra-sensitive nanomechanical mass and force detection [21].

We consider two parallel, flexural nanomechanical resonators, each with an intrinsic Duffing nonlinearity and with a switchable, electrostatically actuated beamsplitter-like coupling between them. The measurement proceeds as follows: one nanoresonator is excited into a large-amplitude coherent state, the beamsplitter interaction is pulsed on so that the coherent-state excitation is split equally between the two resonators, the nanoresonators evolve independently under the nonlinearities (and standard linear dissipation), the beamsplitter interaction is pulsed in the same way again, and a homodyne measurement of the nanoresonator quadratures is performed. As depicted in figure 1, this scheme effectively realizes a nonlinear interferometer [22]. We have calculated the precision with which such a scheme can estimate the nonlinear coefficient of one nanoresonator and demonstrated that the precision scales as $1/n^{3/2}$, where n is the mean phonon number of the initial coherent state.

2. System properties and Hamiltonian

Each nanoresonator can be regarded as a thin bar of length l and lateral width a. We are interested in the fundamental mode of vibration of each nanoresonator in the lateral direction. Each fundamental mode is described by a position–momentum pair, x_i–p_i, where $i = a, b$ labels the resonators. With a time-dependent capacitive coupling dependent on the displacements from

the equilibrium positions, $C(x_a, x_b)$, and Duffing nonlinearities characterized by coefficients χ_i, $i = a, b$, the system can be described classically by a Hamiltonian

$$H_{\rm cl} = \tfrac{1}{2}m\omega^2 x_a^2 + \tfrac{p_a^2}{2m} + \tfrac{1}{2}m\omega^2 x_b^2 + \tfrac{p_b^2}{2m} + P(t)\tfrac{1}{2}C(x_a, x_b)V_0^2 + \tfrac{1}{4}\chi_a m\omega^2 x_a^4 + \tfrac{1}{4}\chi_b m\omega^2 x_b^4 \,, \tag{1}$$

where $P(t)$ specifies the coupling voltage pulses.

In current experiments, the nonlinear coefficient χ of a nanoresonator is estimated [10] by measuring the critical amplitude $a_{\rm c}$ at which the forced oscillations become bistable [23] and the quality factor Q of the oscillator and then using the relation $\chi = 2\sqrt{3}/9a_{\rm c}^2 Q$. Achievable values of these parameters are $a_{\rm c} = 0.7\,{\rm nm}$ and $Q = 20\,000$, giving a nonlinear coefficient $\chi = 4 \times 10^{13}\,{\rm m}^{-2}$. We use this value of χ as a typical value in the following.

We assume that the nanoresonators are capacitively coupled to nearby bias conducting surfaces in such a way that for small displacements, the capacitance can be expanded as

$$C(x_a, x_b) = C_0\left(1 + \frac{f x_a^2 + f x_b^2 + 2x_a x_b}{d^2} + \cdots\right). \tag{2}$$

Here C_0 is the capacitance when the oscillators are at their equilibrium positions. The capacitive coupling must be balanced so that there is no net force on the resonators when the coupling is switched on (i.e. no linear terms in the expansion). This leaves the quadratic terms as the dominant effect of the coupling. In the quadratic terms, $d \simeq 100\,{\rm nm}$ is a characteristic lateral separation between the resonators and the other conducting surfaces and f is a factor of order unity. Both d and f depend on the specific design of the capacitive coupling. Provided

$$C_0 V_0^2/2m\omega d^2 \equiv \kappa \ll \omega \,, \tag{3}$$

we can neglect the renormalization of the resonator frequencies during the pulsing of the capacitive coupling, retaining only the coupling between the resonators. With these assumptions, the capacitive term in the Hamiltonian (1) can be replaced by $P(t)C_0 V_0^2 x_a x_b/d^2$, which gives rise to the desired beamsplitter coupling. The parameter κ, introduced in equation (3), characterizes the strength of the beamsplitter coupling.

Now we quantize by introducing the operators

$$\hat{x}_a = (a + a^\dagger)\sqrt{\frac{\hbar}{2m\omega}} \,, \qquad \hat{p}_a = -{\rm i}(a - a^\dagger)\sqrt{\frac{\hbar m\omega}{2}} \tag{4}$$

satisfying the usual commutation relations, and similarly for nanoresonator b. Transforming to an interaction picture and using the rotating-wave approximation, we find

$$H = \hbar\gamma(a^\dagger a)^2 + \hbar\beta(b^\dagger b)^2 + \hbar\kappa P(t)(a^\dagger b + a b^\dagger) \,, \tag{5}$$

where

$$\gamma \equiv \tfrac{3}{4}\omega\chi_a(\Delta x)^2 \,, \qquad \beta \equiv \tfrac{3}{4}\omega\chi_b(\Delta x)^2 \,, \tag{6}$$

with $\Delta x = \sqrt{\hbar/2m\omega}$ being the half-width of the ground-state wave function. The use of the rotating-wave approximation requires that the timescale δt over which the coupling is varied in $P(t)$ be significantly longer than the periods of the nanomechanical resonators. Since $\delta t \simeq \kappa^{-1}$, this is the requirement, already introduced in equation (3), that $\kappa \ll \omega$.

At low temperatures, nanoresonator damping is thought to be mostly due to coupling to a bath of two-level systems, but this mechanism is not fully understood. Therefore we do not try

to model this mechanism, but rather treat dissipation using a quantum optics master equation (with a zero-temperature bath), with the expectation that this generic model of damping provides a reasonable account of the effect of dissipation on parameter estimation. Then the evolution of the density matrix describing the state of the two nanoresonators is given by

$$\dot{\rho}(t) = -\frac{\mathrm{i}}{\hbar}[H, \rho] + \frac{\Gamma_a}{2}(2a\rho a^\dagger - a^\dagger a\rho - \rho a^\dagger a) + \frac{\Gamma_b}{2}(2b\rho b^\dagger - b^\dagger b\rho - \rho b^\dagger b)\,. \tag{7}$$

Experimentally reasonable values for the system properties are $l = 2\,\mu$m, $a = 40$ nm, $m = 10^{-17}$ kg, $\omega = 2\pi \times 15$ MHz $= 9.4 \times 10^7$ rad s^{-1}, $d = 120$ nm, $Q = 20\,000$, $\chi = 4 \times 10^{13}$ m^{-2}, $C_0 = 10$ aF, and $V_0 = 1$ V. These correspond to $\Delta x = 240$ fm, $\Gamma_i = 4\,700$ s^{-1}, $\gamma, \beta = 1.6 \times 10^{-4}$ s^{-1} (we use 10^{-4} s^{-1} as a typical value in the following), and $\kappa = 3.7 \times 10^5$ s^{-1}. The quantity $1/2\chi(\Delta x)^2 = 5 \times 10^{11}$ is roughly the number of phonons required to make the quartic nonlinearity as large as the harmonic potential; it corresponds to an oscillation amplitude $1/\sqrt{\chi} = 200$ nm. The quality factor and resonant frequency of a nanomechanical resonator have been measured to exhibit a weak temperature dependence [24]. The assumption of a zero temperature bath does not, however, constrain us to the use of 'zero temperature' parameters for our generic model of dissipation. The parameters listed here correspond to values accessible in experiments.

In section 4, we analyze estimation of the nonlinear coefficient γ of oscillator a, assuming that oscillator b has no nonlinearity ($\beta = 0$). Other operating conditions are possible and yield similar results, but the figures in the remainder of the paper refer to the $\beta = 0$ case. We consider a fiducial evolution time $t = 10^{-3}$ s, so that $\Gamma_i t = 4.7$, meaning that the effects of dissipation are large, but not overwhelming, and we consider a fiducial initial phonon number $n = 10^7$, so that the nonlinear phase shift $n\gamma t$ is about 1 rad. We investigate values within about an order of magnitude of these fiducial values. Notice that a phonon number $n = 10^7$ corresponds to an oscillation amplitude $\Delta x\sqrt{2n} = 1$ nm. This amplitude is close to the value we assumed for a_c, not by accident, but because the two oscillation amplitudes quantify, one for free oscillations and one for forced oscillations, the same measure of the relative strengths of the nonlinearity and the damping.

Our assumptions about the switchable beamsplitter coupling require that $\kappa \ll \omega$, so that we can make the rotating-wave approximation, and that $t \gg \kappa^{-1} = 2.7\,\mu$s, so that we can regard the beamsplitter pulses as essentially instantaneous. Both of these inequalities are well satisfied by the above values.

3. System evolution in the *Q* representation

Now suppose that nanoresonator a is excited into a coherent state with amplitude α_0, assumed real. The (product) state of the two nanoresonators is then given, in the Q representation [25], by $Q(\alpha, \alpha^*; t = 0) = \mathrm{e}^{-|\alpha-\alpha_0|^2}/\pi$ and $Q(\beta, \beta^*; t = 0) = \mathrm{e}^{-|\beta|^2}/\pi$. If we pulse on the beamsplitter interaction for a time $\delta t = \pi/4\kappa$, the state of the system is a product of two equal-amplitude coherent states; in other words, we have a 'balanced' beamsplitter. The pulse time δt is sufficiently short that the effect of nonlinearities and dissipation are negligible. We then have

$$Q(\alpha, \alpha^*; t = \delta t) = \frac{1}{\pi}\,\mathrm{e}^{-|\alpha-\alpha_0/\sqrt{2}|^2}\,, \qquad Q(\beta, \beta^*; t = \delta t) = \frac{1}{\pi}\,\mathrm{e}^{-|\beta-\alpha_0/\sqrt{2}|^2}. \tag{8}$$

Setting $P(t) = 0$ in equation (5) for the time between the beamsplitter pulses, the master equation (7) can be converted into a Fokker–Planck equation for the Q function and solved to give [26]

$$Q(\alpha, \alpha^*; t) = \frac{e^{-|\alpha|^2}}{\pi} \sum_{p,q=0}^{\infty} \frac{1}{p!\,q!} \left(\frac{\alpha^* \alpha_0}{\sqrt{2}}\right)^p \left(\frac{\alpha \alpha_0^*}{\sqrt{2}}\right)^q f_a(t)^{(p+q)/2} \exp\left[-|\alpha_0|^2 \frac{f_a(t) + i\delta_a}{2(1 + i\delta_a)}\right], \tag{9}$$

$$Q(\beta, \beta^*; t) = \frac{e^{-|\beta|^2}}{\pi} \sum_{p,q=0}^{\infty} \frac{1}{p!\,q!} \left(\frac{\beta^* \alpha_0}{\sqrt{2}}\right)^p \left(\frac{\beta \alpha_0^*}{\sqrt{2}}\right)^q f_b(t)^{(p+q)/2} \exp\left[-|\alpha_0|^2 \frac{f_b(t) + i\delta_b}{2(1 + i\delta_b)}\right], \tag{10}$$

where

$$\delta_a = 2\gamma(p - q)/\Gamma_a, \quad \delta_b = 2\beta(p - q)/\Gamma_b, \tag{11}$$

$$f_a(t) = \exp[-\Gamma_a t - 2i\gamma t(p - q)], \quad f_b(t) = \exp[-\Gamma_b t - 2i\beta t(p - q)]. \tag{12}$$

The beamsplitter interaction is pulsed on again for time δt, giving output quadratures

$$X_\pm = \frac{a + a^\dagger \pm b \pm b^\dagger}{\sqrt{2}}, \qquad Y_\pm = -\frac{i(a - a^\dagger \pm b \mp b^\dagger)}{\sqrt{2}}. \tag{13}$$

We can calculate the first and second moments of these quadratures using equations (9) and (10),

$$\langle X_\pm \rangle = \sqrt{2} \int d^2\alpha\, \mathcal{R}e(\alpha) Q(\alpha, \alpha^*; t) \pm \sqrt{2} \int d^2\beta\, \mathcal{R}e(\beta) Q(\beta, \beta^*; t), \tag{14}$$

$$\langle X_\pm^2 \rangle = -1 + 2 \int d^2\alpha\, [\mathcal{R}e(\alpha)]^2 Q(\alpha, \alpha^*; t) + 2 \int d^2\beta\, [\mathcal{R}e(\beta)]^2 Q(\beta, \beta^*; t)$$

$$\pm 4 \int d^2\alpha\, \mathcal{R}e(\alpha) Q(\alpha, \alpha^*; t) \int d^2\beta\, \mathcal{R}e(\beta) Q(\beta, \beta^*; t). \tag{15}$$

Corresponding moments of the conjugate quadratures $Y_\pm$ are given by the same expressions with the replacement $\mathcal{R}e(\alpha) \to \mathcal{I}m(\alpha)$.

The evaluation of these moments reduces to the calculation of two integrals,

$$\sqrt{2} \int d^2\alpha\, \alpha\, Q(\alpha, \alpha^*; t) = \sqrt{n} e^{-(\Gamma_a t + nC_2)/2} e^{i(\gamma t + nD_2/2)}, \tag{16}$$

$$2 \int d^2\alpha\, [\mathcal{C}(\alpha)]^2 Q(\alpha, \alpha^*; t) = 1 + \frac{n}{2} e^{-\Gamma_a t} \pm \frac{n}{2} e^{-\Gamma_a t - nC_4/2} \cos(4\gamma t + nD_4/2), \tag{17}$$

where $n = \alpha_0^2$, $\mathcal{C}(\alpha) = \mathcal{R}e(\alpha)$ for the upper sign and $\mathcal{C}(\alpha) = \mathcal{I}m(\alpha)$ for the lower sign, and

$$C_r = C_r(\gamma, \Gamma_a, t) = \frac{1}{1 + (\Gamma_a/r\gamma)^2} \left[1 - e^{-\Gamma_a t} \cos r\gamma t - \frac{\Gamma_a}{r\gamma} e^{-\Gamma_a t} \sin r\gamma t\right], \tag{18}$$

$$D_r = D_r(\gamma, \Gamma_a, t) = \frac{1}{1 + (\Gamma_a/r\gamma)^2} \left[\frac{\Gamma_a}{r\gamma} + e^{-\Gamma_a t} \sin r\gamma t - \frac{\Gamma_a}{r\gamma} e^{-\Gamma_a t} \cos r\gamma t\right]. \tag{19}$$

The general results are complicated and thus are not quoted here. In the case of no damping ($\Gamma_a = 0 = \Gamma_b$), we can show that

$$\langle X_\pm \rangle = \sqrt{n}\mathrm{e}^{-n(1-\cos 2\gamma t)/2}\cos\left(\gamma t + \frac{n}{2}\sin 2\gamma t\right) \pm \sqrt{n}\mathrm{e}^{-n(1-\cos 2\beta t)/2}\cos\left(\beta t + \frac{n}{2}\sin 2\beta t\right), \quad (20)$$

$$\langle Y_\pm \rangle = \sqrt{n}\mathrm{e}^{-n(1-\cos 2\gamma t)/2}\sin\left(\gamma t + \frac{n}{2}\sin 2\gamma t\right) \pm \sqrt{n}\mathrm{e}^{-n(1-\cos 2\beta t)/2}\sin\left(\beta t + \frac{n}{2}\sin 2\beta t\right), \quad (21)$$

and

$$\begin{aligned}\langle X_\pm^2 \rangle = 1 + n &+ \frac{n}{2}\mathrm{e}^{-n(1-\cos 4\gamma t)/2}\cos\left(4\gamma t + \frac{n}{2}\sin 4\gamma t\right) + \frac{n}{2}\mathrm{e}^{-n(1-\cos 4\beta t)/2}\cos\left(4\beta t + \frac{n}{2}\sin 4\beta t\right) \\ &\pm n\mathrm{e}^{-n(2-\cos 2\gamma t-\cos 2\beta t)/2}\cos\left(\gamma t - \beta t + \frac{n}{2}\sin 2\gamma t - \frac{n}{2}\sin 2\beta t\right) \\ &\pm n\mathrm{e}^{-n(2-\cos 2\gamma t-\cos 2\beta t)/2}\cos\left(\gamma t + \beta t + \frac{n}{2}\sin 2\gamma t + \frac{n}{2}\sin 2\beta t\right), \end{aligned} \quad (22)$$

$$\begin{aligned}\langle Y_\pm^2 \rangle = 1 + n &- \frac{n}{2}\mathrm{e}^{-n(1-\cos 4\gamma t)/2}\cos\left(4\gamma t + \frac{n}{2}\sin 4\gamma t\right) - \frac{n}{2}\mathrm{e}^{-n(1-\cos 4\beta t)/2}\cos\left(4\beta t + \frac{n}{2}\sin 4\beta t\right) \\ &\pm n\mathrm{e}^{-n(2-\cos 2\gamma t-\cos 2\beta t)/2}\cos\left(\gamma t - \beta t + \frac{n}{2}\sin 2\gamma t - \frac{n}{2}\sin 2\beta t\right) \\ &\mp n\mathrm{e}^{-n(2-\cos 2\gamma t-\cos 2\beta t)/2}\cos\left(\gamma t + \beta t + \frac{n}{2}\sin 2\gamma t + \frac{n}{2}\sin 2\beta t\right). \end{aligned} \quad (23)$$

Note that these results could have been calculated directly in the Heisenberg picture with initial coherent states in each mode. Making, in addition, the *short-time approximation*, $n(\gamma t)^2, n(\beta t)^2 \ll 1$, which still allows nonlinear phase shifts $n\gamma t$ and $n\beta t$ much larger than unity, we find the same expectation values as for the analogous classical nonlinear interferometer:

$$\langle X_\pm \rangle \to \sqrt{n}\cos n\gamma t \pm \sqrt{n}\cos n\beta t\,, \quad \langle Y_\pm \rangle \to \sqrt{n}\sin n\gamma t \pm \sqrt{n}\sin n\beta t\,. \quad (24)$$

We can define a regime of strong damping by the conditions

$$\frac{\Gamma_a}{\gamma}, \frac{\Gamma_b}{\beta} \gg \sqrt{n}\,, \quad \gamma t, \frac{\Gamma_a t}{n}, \frac{\Gamma_b t}{n} \ll 1\,. \quad (25)$$

The conditions on the evolution time are of little consequence because long before they are violated, the oscillators will have damped to the ground state. Notice that these conditions allow the case of most interest to us, i.e. $\Gamma_b = \Gamma_a \simeq \gamma n$, with $n\gamma t \simeq \Gamma_a t$ allowed to be considerably larger than unity. In the strong damping regime, we have

$$\langle X_\pm \rangle = \sqrt{n}\mathrm{e}^{-\Gamma_a t/2}\cos\left[\frac{n\gamma}{\Gamma_a}(1-\mathrm{e}^{-\Gamma_a t})\right] \pm \sqrt{n}\mathrm{e}^{-\Gamma_b t/2}\cos\left[\frac{n\beta}{\Gamma_b}(1-\mathrm{e}^{-\Gamma_b t})\right], \quad (26)$$

$$\langle Y_\pm \rangle = \sqrt{n}\mathrm{e}^{-\Gamma_a t/2}\sin\left[\frac{n\gamma}{\Gamma_a}(1-\mathrm{e}^{-\Gamma_a t})\right] \pm \sqrt{n}\mathrm{e}^{-\Gamma_b t/2}\sin\left[\frac{n\beta}{\Gamma_b}(1-\mathrm{e}^{-\Gamma_b t})\right]. \quad (27)$$

In addition, in this regime $\langle X_\pm^2 \rangle = 1 + \langle X_\pm \rangle^2$ and $\langle Y_\pm^2 \rangle = 1 + \langle Y_\pm \rangle^2$, which means that the quadrature uncertainties are at the coherent-state level, i.e. $\Delta X_\pm = \Delta Y_\pm = 1$.

The dependence of the expectation values of the '+' quadrature amplitudes on the nonlinearity and damping rate is shown in figure 2; similar behavior is displayed by the '−' quadratures. The nonlinearity gives rise to rapidly oscillating fringes, and this is the key, as we see in the following section, to the enhanced sensitivity of the nonlinear interferometer.

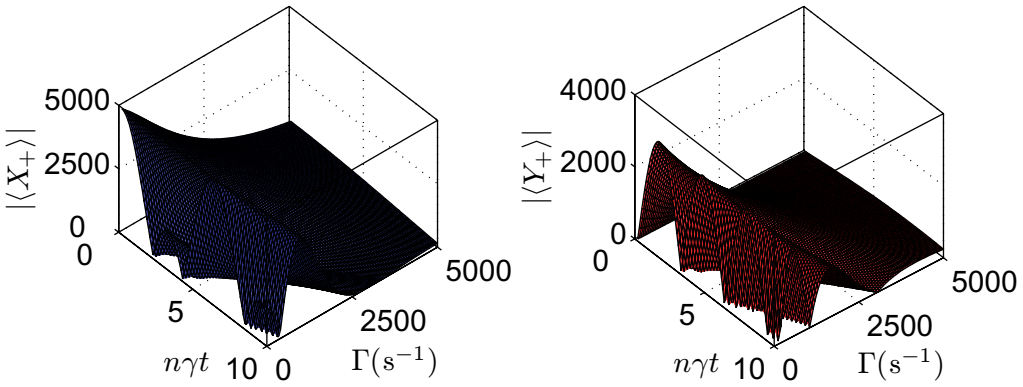

Figure 2. Magnitude of expectation values of output quadratures X_+ and Y_+ as functions of the nonlinearity γ (expressed in terms of the nonlinear phase shift $n\gamma t$) and nanoresonator damping $\Gamma(=\Gamma_a=\Gamma_b)$, for the choices $n=10^7$, $\beta=0$ and $t=10^{-3}$ s. The rapidly oscillating fringes with respect to γ give rise to the enhanced sensitivity of this parameter estimation scheme. Damping leads to a shift in the location of the fringes and to a decay of the quadrature expectations.

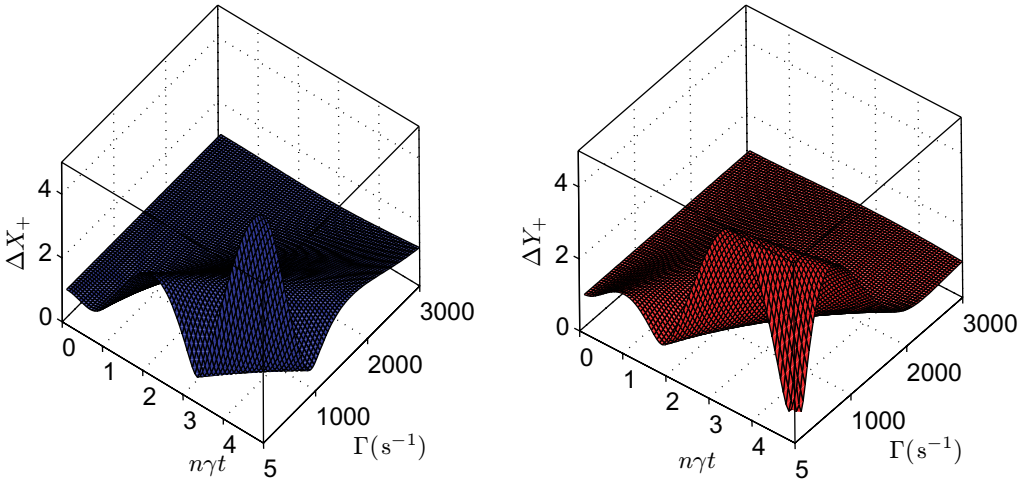

Figure 3. Uncertainty in the output quadratures X_+ and Y_+ as a function of the nonlinearity γ (expressed in terms of the nonlinear phase shift $n\gamma t$) and nanoresonator damping $\Gamma(=\Gamma_a=\Gamma_b)$, for the choices $n=10^7$, $\beta=0$, and $t=10^{-3}$ s. Squeezing and anti-squeezing are observed for low damping, corresponding to shearing of the contours of the Q function in phase space. Dissipation suppresses this effect, and coherent-state variances, corresponding to decay to the vacuum, are seen at high damping rates.

Dissipation leads to a reduction in the expectation values and also to a reduction in the fringe frequency. Figure 3 shows the uncertainties in X_+ and Y_+, also as functions of the nonlinearity and damping rate. In the case of low damping, as the nonlinear phase shift increases, the variances oscillate, corresponding to the shearing apart and partial recurrence of the contours of the Q function in phase space. Squeezing and anti-squeezing are apparent in the variance

oscillations [27], and the squeezing can be quite substantial. (Achieving *quantum* squeezing is quite difficult for reasonable damping rates and would be made even more so by a finite-temperature bath.) Damping suppresses the shearing—and, hence the squeezing and anti-squeezing—and suppresses the quantum interference effects that give rise to partial revivals. Strong damping leads to a decay of the expectation values and to quadrature variances that take on the coherent-state value. At reasonable damping rates, we cannot derive any benefit from the squeezing, though neither are we adversely affected by the anti-squeezing of the quadratures. The deleterious effect of damping is almost entirely a consequence of reducing the signal carried by the expectation values, not of changing the variances.

4. Precision of parameter estimate

To analyze the precision of estimating the strength of the Duffing nonlinearity, we specialize in this section to the case where oscillator b has no nonlinearity ($\beta = 0$). We are thus estimating the nonlinear coefficient γ of oscillator a. Other operating conditions are possible, but we focus on this one as a representative possibility in this section.

We phrase our results in terms of the precision in estimating the related dimensionless parameter γt, with t regarded as fixed. The uncertainty in an estimate of γt based on multiple measurements of a quantity Z—in our case, Z is one of the output quadratures—can be calculated from

$$\delta(\gamma t) = t\delta\gamma = t\frac{\Delta Z}{|\mathrm{d}\langle Z\rangle/\mathrm{d}\gamma|} = \frac{\Delta Z}{|\mathrm{d}\langle Z\rangle/\mathrm{d}(\gamma t)|}\,, \tag{28}$$

where ΔZ is the uncertainty in Z. In the case of no damping and again making the short-time approximation, the quadrature variances all take on coherent-state values, i.e. $\Delta X_\pm$, $\Delta Y_\pm \to 1$. The precision of the estimate of γt thus becomes

$$\delta_{X_\pm}(\gamma t) = \frac{1}{n^{3/2}|\sin n\gamma t|}\,, \qquad \delta_{Y_\pm}(\gamma t) = \frac{1}{n^{3/2}|\cos n\gamma t|}\,. \tag{29}$$

These sensitivities oscillate with the fringes produced by the nonlinear phase shift $n\gamma t$, but they all have the same basic scaling of $1/n^{3/2}$ with phonon number. This scaling beats the $1/n$ scaling achievable with a linear Hamiltonian and is consistent with the general result [6] for nonlinear Hamiltonians and initial product states. The factor of n enhancement compared with the standard quantum limit for linear Hamiltonians is a consequence of the rapidly oscillating fringes in the expectation values of the output quadratures.

From an experimental perspective, the strong damping regime (25) is most relevant. In this regime, the quadrature variances have coherent-state values, and the derivatives of the expectation values lead to sensitivities

$$\begin{aligned}
\delta_{X_\pm}(\gamma t) &= \frac{\Gamma_a t\, \mathrm{e}^{\Gamma_a t/2}}{n^{3/2}(1-\mathrm{e}^{-\Gamma_a t})|\sin[n\gamma(1-\mathrm{e}^{-\Gamma_a t})/\Gamma_a]|}\,,\\
\delta_{Y_\pm}(\gamma t) &= \frac{\Gamma_a t\, \mathrm{e}^{\Gamma_a t/2}}{n^{3/2}(1-\mathrm{e}^{-\Gamma_a t})|\cos[n\gamma(1-\mathrm{e}^{-\Gamma_a t})/\Gamma_a]|}\,.
\end{aligned} \tag{30}$$

The improved $1/n^{3/2}$ sensitivity scaling survives in the presence of dissipation, but the absolute sensitivity is degraded, and the fringes become more widely separated. For feasible damping rates, the sensitivity is worsened by less than an order of magnitude, but if the damping is further

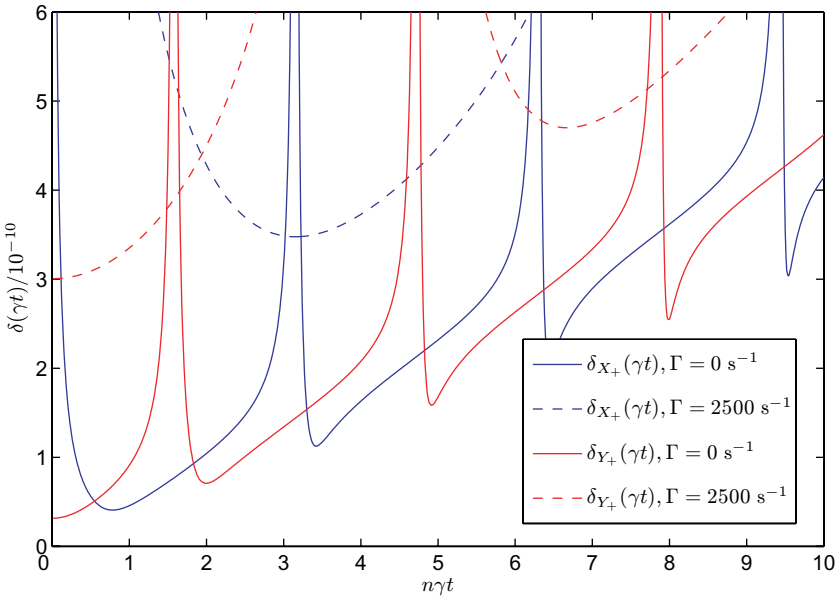

Figure 4. Precision $\delta(\gamma t)$ for measurements of the X_+ and Y_+ quadratures as a function of the nonlinearity γ, expressed as the nonlinear phase shift $n\gamma t$, for the choices $n = 10^7$, $\beta = 0$, $t = 10^{-3}$ s, and $\Gamma_a = \Gamma_b = \Gamma$. Zero damping and moderate damping cases are shown for each quadrature. For zero damping, fringe boundaries are located at $n\gamma t = m\pi/2$, with the fringes based on measurements of conjugate quadratures displaced by $\pi/2$. Dissipation leads to an overall reduction in sensitivity, and the fringes become more widely spaced.

increased, the sensitivity diverges, reflecting the absence of signal in the quadrature expectation values.

Figure 4 shows the measurement precision for measurements of the X_+ and Y_+ quadratures as a function of the nonlinearity γ and for two values of the damping rate $\Gamma = \Gamma_a = \Gamma_b$. Fringe boundaries are located at $n\gamma t = m\pi/2$; those based on measurement of the X_+ and Y_+ quadratures are displaced by $\pi/2$. As the damping rate increases, the overall sensitivity worsens, and the fringes become more widely spaced. These effects can be traced back to the reduced-amplitude and reduced-frequency oscillations of the quadrature expectations as a function of the nonlinear phase shift.

The scaling of the measurement precision as a function of n is plotted in figure 5. Here n is chosen so that $n\gamma t < 1$. The precision associated with measurement of the Y_+ quadrature is then near its optimal value, away from its first fringe boundary at $n\gamma t = \pi/2$, whereas the precision associated with measurement of the X_+ quadrature decreases rapidly as it falls from the very poor sensitivity near its central fringe boundary at $n\gamma t = 0$. From the log–log plot, we can calculate that $\delta_{X_+} \propto n^{-5/2}$ and $\delta_{Y_+} \propto n^{-3/2}$, though the extra n^{-1} in the $n^{-5/2}$ scaling is due to the sensitivity falling from the central fringe boundary, and the true scaling of the optimal sensitivity achievable is $n^{-3/2}$. The scaling behavior is maintained in the presence of feasible levels of dissipation, although there is a marked deterioration in sensitivity.

In practice, the initial state of the excited nanoresonator would be better described by a displaced thermal state. Provided that the thermal width of this state is small compared with the

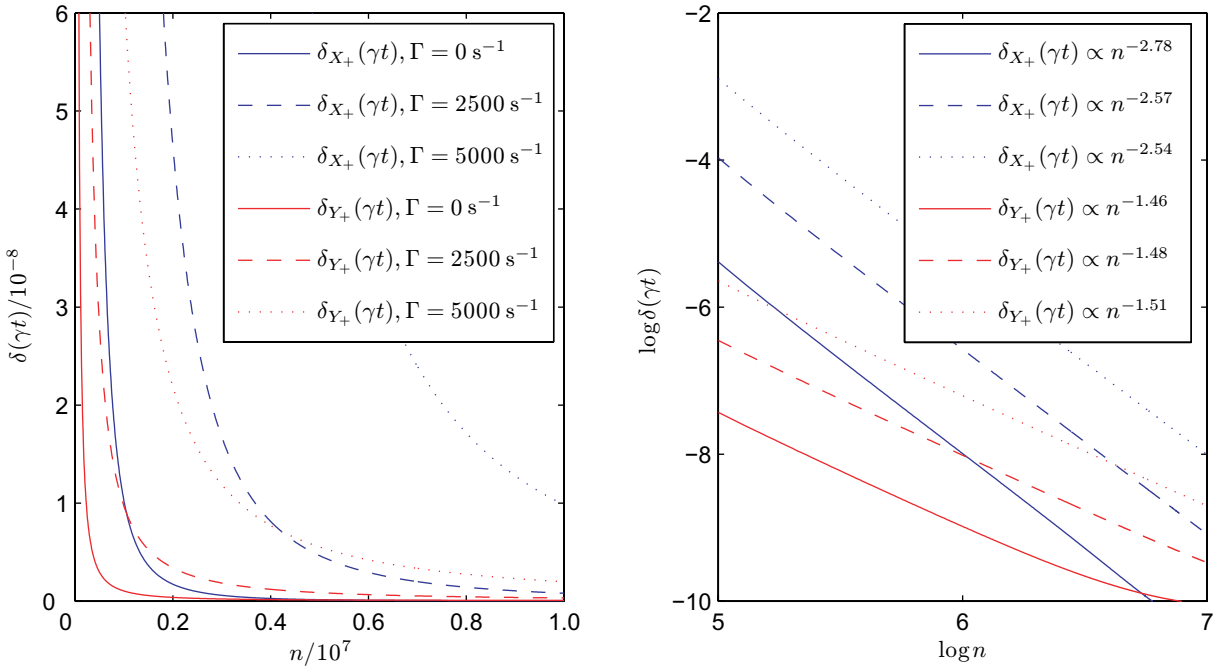

Figure 5. Precision $\delta(\gamma t)$ for measurements of the X_+ and Y_+ quadratures as a function of mean phonon number n in the initial coherent state, for the choices $\gamma = 10^{-4}\ \mathrm{s}^{-1}$, $\beta = 0$, $t = 10^{-3}$ s and $\Gamma_a = \Gamma_b = \Gamma$. Plots for three values of the damping constant Γ are shown for each quadrature. These plots correspond to the regime $n\gamma t < 1$. From the log–log plots, we see that $\delta_{X_+} \propto n^{-5/2}$ and $\delta_{Y_+} \propto n^{-3/2}$. The extra n^{-1} factor for measurement of the X_+ quadrature is due to the precision improving as one moves away from the very poor sensitivity near the central fringe boundary.

amplitude of the displacement, a condition that would be well satisfied by an excitation at the level we are considering, the primary effect of an initial thermal distribution would be simply to increase the output quadrature variances, leading to a reduction in sensitivity, but not to change in the scaling behavior. In the strong damping regime, contact with a finite temperature bath would result in thermal rather than coherent-state variances in the output quadratures, again leading to a reduction in sensitivity, but not to a change in the scaling with n. Note that the quantum optics master equation for the nonlinearities we consider and with a finite temperature bath has been solved analytically using the Q representation [28]. We conclude that the measurement scheme we describe is reasonably robust to increases in temperature. A more severe difficulty lies in performing quantum-limited homodyne detection of the output quadratures, though it is conceivable that such measurements could be performed using coupled microwave cavities [29].

5. Conclusions

We have calculated the precision with which the nonlinearity of a nanomechanical resonator can be estimated, using a nanomechanical analogue of a nonlinear interferometer. For an input

coherent state, the precision scales as $1/n^{3/2}$, a scaling beyond that achievable with a linear coupling even when entangled input states are employed. This scaling behavior is maintained in the presence of dissipation, which we modeled using a quantum optics master equation, and it is expected that this scheme is reasonably robust to increases in temperature. Quantum-limited homodyne detection of the nanoresonator quadratures is, however, a very challenging experimental task.

An alternative scheme would use a single nonlinear nanomechanical resonator coupled to the field in a superconducting microwave cavity, which would act as the second 'arm' of an interferometer. The nonlinearity would then only be in the mechanical arm of the interferometer. The initial state would be excited by driving the cavity, and readout would be performed by quantum-limited homodyne detection of the cavity output. A beamsplitter-like interaction between the cavity and nanoresonator could be realized by driving the cavity on its red sideband [30]. This beamsplitter coupling would be continuous, so the analytical results obtained here are not directly applicable. Investigating the achievable sensitivity of this cavity–nanoresonator scheme is the subject of ongoing work.

Acknowledgments

We thank A C Doherty for useful discussions. This work was supported in part by the Australian Research Council and by the US Office of Naval Research grant no. N00014-07-07-1-0304.

References

[1] Helstrom C W 1976 *Quantum Detection and Estimation Theory* (New York: Academic)
[2] Diddams S A, Bergquist J C, Jefferts S R and Oates C W 2004 *Science* **306** 1318
[3] Giovannetti V, Lloyd S and Maccone L 2006 *Phys. Rev. Lett.* **96** 010401
[4] Giovannetti V, Lloyd S and Maccone L 2004 *Science* **306** 1330
[5] Boixo S, Flammia S T, Caves C M and Geremia J M 2007 *Phys. Rev. Lett.* **98** 090401
[6] Boixo S, Datta A, Flammia S T, Shaji A, Bagan E and Caves C M 2008 *Phys. Rev.* A **77** 012317
[7] Higgins B L, Berry D W, Bartlett S D, Wiseman H M and Pryde G J 2007 *Nature* **450** 393
[8] Rudolph T and Grover L 2003 *Phys. Rev. Lett.* **91** 217905
[9] de Burgh M and Bartlett S D 2005 *Phys. Rev.* A **72** 042301
[10] Kozinsky I, Postma H W Ch, Kogan O, Husain A and Roukes M L 2007 *Phys. Rev. Lett.* **99** 207201
[11] Teufel J D, Regal C A and Lehnert K W 2008 *New J. Phys.* **10** 094002
[12] Luis A 2004 *Phys. Lett.* A **329** 8
[13] Beltrán J and Luis A 2005 *Phys. Rev.* A **72** 045801
[14] Luis A 2007 *Phys. Rev.* A **76** 035801
[15] Partner H L, Black B D and Geremia J M 2007 arXiv: 0708.2730 [quant-ph]
[16] Rey A M, Jiang L and Lukin M D 2007 *Phys. Rev.* A **76** 053617
[17] Choi S and Sundaram B 2008 *Phys. Rev.* A **77** 053613
[18] Boixo S, Datta A, Davis M J, Flammia S T, Shaji A and Caves C M 2008 *Phys. Rev. Lett.* **101** 040403
[19] Carr S M, Lawrence W E and Wybourne M N 2001 *Phys. Rev.* B **64** 220101
[20] Aikele M, Bauer K, Ficker W, Neubauer F, Prechtel U, Schalk J and Seidel H 2001 *Sensors Actuators* A **92** 161
[21] Aldridge J S and Cleland A N 2005 *Phys. Rev. Lett.* **94** 156403
[22] Kitagawa M and Yamamoto Y 1986 *Phys. Rev.* A **34** 3974
[23] Nayfeh A H and Mook D T 1979 *Nonlinear Oscillations* (New York: Wiley)

[24] Zolfagarkhani G, Gaidarzhy A, Shim S-B, Badzey R L and Mohanty P 2005 *Phys. Rev.* B **72** 224101
[25] Milburn G J and Walls D F 2008 *Quantum Optics* (Berlin: Springer)
[26] Milburn G J and Holmes C A 1986 *Phys. Rev. Lett.* **56** 2237
[27] Milburn G J 1986 *Phys. Rev.* A **33** 674
[28] Daniel D J and Milburn G J 1989 *Phys. Rev.* A **39** 4628
[29] Regal C A, Teufel J D and Lehnert K W 2008 *Nat. Phys.* **4** 555
[30] Woolley M J, Doherty A C, Milburn G J and Schwab K C 2008 arXiv: 0803.1757 [quant-ph]